Thermal Properties of Deuterium Oxide near the Triple Point Predicted from Nonequilibrium Evaporation

Fei Duan,* A. Crivoi, and B. He

Division of Thermal and Fluids Engineering, School of Mechanical and Aerospace Engineering, Nanyang Technological University, Singapore 639798

Statistical rate theory (SRT) was applied to predict the saturation pressure of D_2O numerically near the triple point based on the interfacial liquid-phase temperature, the interfacial vapor-phase temperature, and the local evaporation flux from 102 local measures in a series of nonequilibrium steady-state droplet evaporation experiments. An analytical expression of the saturation pressure, P_{sat}, was obtained from the predicted values. Following the thermodynamic relations, the specific entropy of evaporation, h_{fg}, and the liquid-phase specific heat at constant pressure, C_p^L, were computed. The agreement that the calculated values of these properties with those obtained from the independent measurements indicates that the SRT expression accurately predicts the thermal properties of D_2O near the triple point.

Introduction

The accurate measurement of thermal properties near the triple point is always a challenge for a liquid due to the possible ice formation. Deuterium oxide, D_2O, a heavy water which has the same structure as H_2O, is normally applied in the operation of nuclear power reactors as a moderator or a heat transfer agent. Solvents created with the heavy water are used to help researchers determine the structure of complex organic chemicals in life science. Additionally and importantly, from the point of view of physics and chemistry, the steady-state experiments near the triple point on evaporating D_2O droplets help us to validate a method to predict the thermal properties (the saturation pressure, P_{sat}, the specific entropy of evaporation or condensation, h_{fg}, and the specific heat at constant pressure in the liquid, C_p^L) on the basis of the statistical rate theory (SRT) approach introduced below. By definition, the saturation pressure, P_{sat}, at its isothermal liquid temperature, is determined at a flat surface under the equilibrium conditions. The pressure of D_2O was experimentally measured above the triple point at 276.97 K,[1−4] whereas the experiments were seldom reported in measuring P_{sat} directly below the triple point. Bottomley measured the vapor-pressure difference between the metastable liquid and the stable solid of D_2O by using two 0.5 g samples in two connected glass bulbs, respectively, as the temperature was lowered to 261.35 K.[5] However, the assumption of thermal equilibrium might be difficult to reach in the experiments. A mass transport was expected due to the pressure difference in the connected tube between the water sample at a higher vapor pressure and the ice sample at a lower vapor pressure during the measurement. The values of P_{sat} reported by Bottomley are plotted in Figure 1 with his smoothed fitting curve. A detectable deviation could be found there. The measurement values are 4.1 % at 2.0 °C and 11.1 % at 261.35 K higher than the fitting curve. Kraus and Greer directly measured the vapor pressure of the metastable liquid D_2O in the range (257.75 to 276.35) K above the small dew droplets condensed from the hot vapor under the assumed equilibrium conditions.[6] They could not directly observe the droplets during the measurement, so some droplets might be frozen at lower temperatures which would affect their readings. The measurements of Kraus and Greer and their fitting equation are plotted in Figure 1 as well. The measured values are also higher than the fitting curve. The difference is 4.6 Pa at 257.75 K, while it is 27.3 Pa at 276.35 K. There is a variation between the two sets of experimental data below the triple point of D_2O. At 261.35 K, the value of P_{sat} reported by Kraus and Greer is 4.7 Pa greater than that of Bottomley.

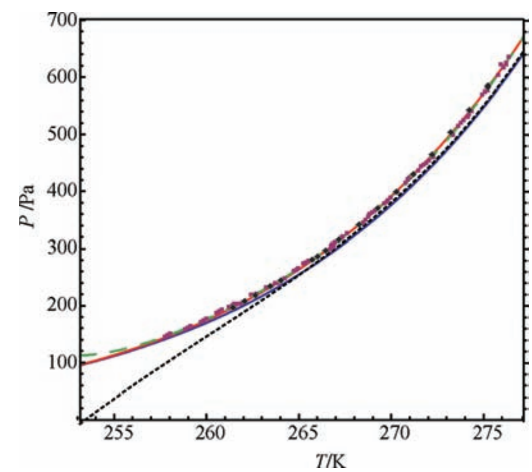

Figure 1. Comparison of the experimental vapor-phase pressures of D_2O with the existing fitting expressions of the saturation pressure from Bottomley (black dotted line),[5] Kraus and Greer (blue solid line),[6] Kraus and Greer (f) (green dashed line),[7] and Pupezin et al. (red solid line).[1] Data from: ■, Kraus and Greer;[6] ◆, Bottomley.[5]

Pupezin et al. provided an empirical saturation pressure equation, $P_{sat,P}$, based on their experimental data for D_2O from (270 to 373) K,[1] which partially covers the metastable range below the triple point. If it is extended into a lower temperature, the equation surprisedly has a close agreement with the data reported by Bottomley[5] within a derivation of 1 %, by Kraus and Greer[6] within a derivation of 3 %. As shown in Figure 2, the difference of the equation in Pupezin et al. from the polynomial fitting of the measures of Kraus and Greer, $P_{sat,KG(f)}$,[7]

* Corresponding author. E-mail: feiduan@ntu.edu.sg.

10.1021/je100226g
Published on Web 06/15/2010

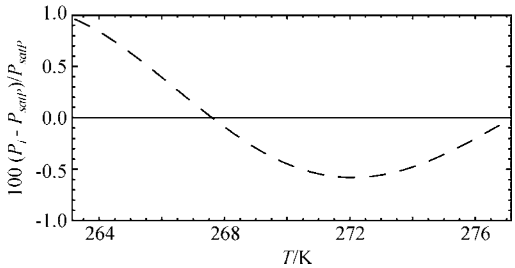

Figure 2. Comparison of the existing fitting expressions of the saturation pressure between the fitting from Kraus and Greer data (dashed line), $P_{sat,KG(f)}$[7] and Pupezin et al. (solid line), $P_{sat,P}$.[1]

is less than 1 % in the measured temperature range; however, a clear offset is demonstrated as the temperature is less than 258 K. But yet, no one can be sure of the validity of the expression given by Pupezin et al. below 270 K since the curve is extrapolated to the temperature region. In addition, the fitting curves by Kraus and Greer and by Bottomley are clearly below the expression of Pupezin et al. Nevertheless, both of the equations of $P_{sat,P}$[1] from Pupezin et al. and the fitting relation of $P_{sat,KG(f)}$[7] from the data of Kraus and Greer were used as a criterion in predicting the saturation pressure from SRT in our numerical analysis, introduced in the Results and Discussion section.

A series of steady-state evaporation experiments of a sessile droplet were conducted above a conical funnel when the global vapor-phase pressure was maintained at a predetermined value from (253.3 to 654.6) Pa. The local interfacial liquid temperature was maintained near the triple point. The temperature discontinuity was found across the liquid−vapor interface at each measured position; the interfacial vapor temperature was greater than that in the liquid phase. The liquid phase was not frozen even though the droplet was disturbed by the moveable thermocouple all of the time in the experiments until the global vapor-phase pressure was reduced below 250 Pa. When the measurements are applied in the SRT approach,[8−15] the saturation pressure can be determined on the basis of the interfacial temperatures, the vapor-phase pressure, the local evaporation flux, and the thermal and molecular properties at each of the measured positions. In the paper, we propose to determine the expression of P_{sat} for D_2O from the measurement made in steady-state nonequilibrium evaporation. The saturation pressure from SRT below the triple point is then formulated and compared with the existing equations given by Pupezin et al.,[1] Jones,[4] Bottomley,[5] Kraus and Greer,[6] Hill and MacMillan,[16] Harvey and Lemmon,[17] and Matsunaga and Nagashima.[18] After, the specific entropy of evaporation, h_{fg}, is calculated from the P_{sat} curves by using the first differential of the saturation equation and compared with the independent measurements[19,20] to reveal the analytical expression of the saturation pressures from SRT better than the other expressions of P_{sat}. Further, as the specific heat at constant pressure of the liquid phase, C_p^L, determined by the second differential of the P_{sat} expressions, is compared with the reported values;[21−25] all of the previous expressions for P_{sat} are in disagreement with the measured data in a wide temperature range.

Experimental Measurement

The detailed experimental equipment and process were reported in refs 7 and 26. Simply speaking, the heavy water (D_2O, minimum isotopic deuterium atom at 0.9992 in mass fraction) was degassed at first in a sealed glass flask. Simultaneously, the experimental chamber and syringe were evacuated

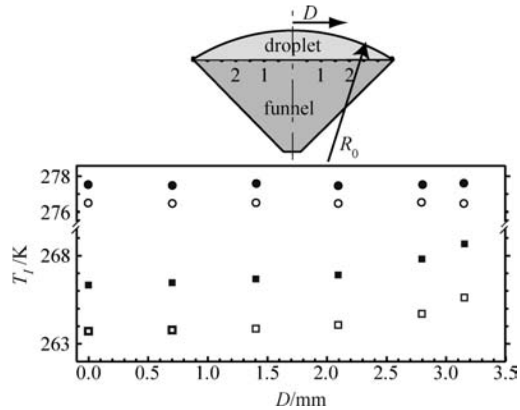

Figure 3. Interfacial liquid and vapor temperature measures across the interface of droplet of D_2O under the steady-state conditions: ●, EVD3 vapor; ○, EVD3 liquid; ■, EVD11 vapor; □, EVD11 liquid. The top diagram is a sketch of the droplet which has a spherical interface with a radius of R_0 if the maximum height of the droplet was maintained at 1.0 mm,[7] and D is the distance from the centerline of the droplet.

Table 1. Experimental Conditions Measured in Steady-State Evaporation of D_2O[7]

	P^V_{global}	R_0	$j_{ev}/(gm^{-2}\cdot s^{-1})$					
			0.0	0.7	1.4	2.1	2.8	3.15
exp.	Pa	mm	mm	mm	mm	mm	mm	mm
EVD1	651.9	6.625	0.059	0.059	0.059	0.059	0.059	0.059
EVD2	654.6	6.740	0.074	0.074	0.074	0.074	0.074	0.074
EVD3	649.3	6.740	0.081	0.081	0.081	0.081	0.081[a]	0.081
EVD4	642.6	6.740	0.087	0.087	0.087	0.087	0.088	0.090
EVD5	625.3	6.625	0.098	0.110	0.141	0.179	0.234	0.291
EVD6	591.9	6.625	0.111	0.148	0.225	0.284	0.414	0.664
EVD7	549.3	6.625	0.199	0.286	0.492	0.697	0.864	1.026
EVD8	450.6	6.625	0.408	0.589	1.067	1.646	2.032	2.093
EVD9	350.6	6.515	0.667	0.966	1.721	2.530	2.828	2.630
EVD10	308.0	6.625	0.764	1.479	2.867	3.350	2.344	1.897
EVD11	253.3	6.569	0.945	1.736	3.281	3.857	2.839	2.455

[a] At 2.7 mm.

to a pressure at about 10^{-5} Pa by turbo and backing mechanical pumps. The droplet was formed on the conical funnel mouth, while the degassed water was transported directly into a syringe mounted on a syringe pump. To prevent subsequent bubble formation in the funnel and tube, the chamber was pressurized before the chamber was dried with the help of an evaporating mechanical pump. The liquid was pumped into the funnel until the maximum height of the liquid−vapor interface above the funnel mouth was approximately 1.0 mm to maintain a spherical interface with a radius (R_0) as shown in the top diagram in Figure 3 and listed in Table 1,[7] monitored with the cathetometers from outside of the evaporation chamber. The temperature at the funnel throat was maintained at 276.85 K to keep the lighter liquid at a lower temperature on the top of the denser liquid in the funnel during evaporation. Under the steady-state conditions, the maximum interface height was maintained with an uncertainty of 10 μm, the liquid pumping speed was controlled at a constant value, and the global vapor-phase pressure (P^V_{global}) was regulated at a value from (253.3 to 654.6) Pa as listed in Table 1. The temperatures in the vapor and liquid phases were measured with a calibrated U-shaped moveable K-type thermocouple (25.4 μm in diameter) and mounted on a three-dimensional positioner, in horizontal directions at (0.0, 0.7, 1.4, 2.1, 2.8, and 3.15) mm from the centerline of the evaporation droplet in the liquid and vapor phases, respectively. At each position, the temperature was recorded for a period of 1 min with one reading per second by a LabView program using a 34970A Agilent data acquisition/switch unit, and the mean and standard deviation of the readings at each point were calculated. As illustrated in Figure 3 for the experiments of EVD3 and EVD11, at each position, the interfacial vapor temperature was found to be greater than the interfacial liquid temperature. This ranged from 1.0 K in the experiment of EVD1 to 2.7 K in the experiment of EVD11. Before the transition of thermocapillary convection,[7,14,27] the interfacial temperature at liquid and vapor phases was roughly uniform; however, the interfacial temperature increased from the centerline to the periphery of the droplet gradually after the transition. The global pressure in the vapor phase measured with the aid of an Hg manometer and the local evaporation flux (j_{ev}) calculated from the energy boundary conditions[7] are listed in Table 1. Subsequently, the interfacial temperatures in the liquid and vapor phases, the local evaporation flux, and the thermal and molecular properties were substituted into the SRT approach to predict the saturation pressure numerically at each measured position in the steady-state evaporation experiments of D_2O.

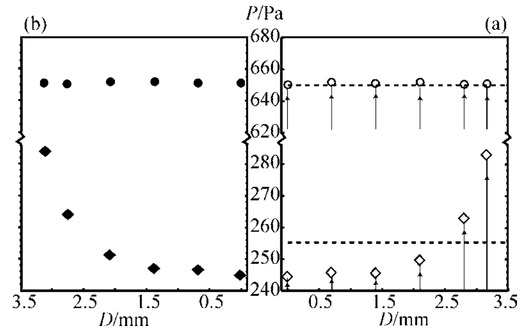

Figure 4. Local predicted pressure as a function of position from the centerline to the periphery of the evaporation droplet. The predicted vapor-phase values from SRT are compared with the global measured vapor-phase pressure in (a): ○, EVD3; ◇, EVD11. The saturated pressure is computed numerically to satisfy the saturation pressure from the formulas in (b): ●, EVD3; ◆, EVD11. The dashed line is the global vapor-phase pressure.

Results and Discussion

Saturation Pressure Prediction from the Evaporation Experiments. The local evaporation flux, j_{ev}, that is obtained from SRT can be expressed in terms of two thermodynamic functions, the equilibrium constant, K_e, and the entropy change, Δs^{LV},

$$j_{ev} = 2K_e \sinh\left(\frac{\Delta s^{LV}}{k_b}\right) \tag{1}$$

where k_b is the Boltzmann constant.

If the local equilibrium is assumed valid in each phase, the function of K_e may be written as

$$K_e = \frac{P_{sat}(T_I^L) \exp\left[\frac{\upsilon_{sat}^L}{k_b T_I^L}(P_e^L - P_{sat}(T_I^L))\right]}{\sqrt{2\pi m_w k_b T_I^L}} \tag{2}$$

where $P_{sat}(T_I^L)$ is the saturated pressure at the interfacial liquid temperature, T_I^L, υ_{sat}^L is the specific volume at the interfacial liquid temperature,[7] and m_w is the molecular weight of the heavy water. As the surface tension is denoted as γ^{LV},[7] P_e^L is determined as the solution of

$$P_e^L = P_{sat}(T_I^L) \exp\left[\frac{\upsilon_{sat}^L(T_I^L)}{k_b T_I^L}(P_e^L - P_{sat}(T_I^L))\right] + \frac{2\gamma^{LV}}{R_0} \tag{3}$$

The function of Δs^{LV} can be simplified as,[8-14]

$$\Delta s^{LV} = k_b\left[4\left(1 - \frac{T_I^V}{T_I^L}\right) + \left(\frac{1}{T_I^V} - \frac{1}{T_I^L}\right)\sum_{l=1}^{3}\left(\frac{\hbar\omega_l}{2k_b} + \frac{\frac{\hbar\omega_l}{k_b}}{\exp\left(\frac{\hbar\omega_l}{k_b T_I^V}\right) - 1}\right) + \frac{\upsilon_{sat}^L}{k_b T_I^L}\left[P_I^V + \frac{2\gamma^{LV}}{R_0} - P_{sat}(T_I^L)\right] + \ln\left[\left(\frac{T_I^V}{T_I^L}\right)^4\left(\frac{P_{sat}(T_I^L)}{P_I^V}\right)\left(\frac{q_{vib}(T_I^V)}{q_{vib}(T_I^L)}\right)\right]\right] \tag{4}$$

where T_I^V is the local interfacial vapor temperature, P_I^V is the local vapor-phase pressure, and q_{vib} is the vibrational partition function in eq 5. The vibrations of the covalent bonds in the heavy water (D_2O) molecule are (1178.38, 2669.4, and 2787.92) cm^{-1}.[28]

$$q_{vib}(T) = \prod_{l=1}^{3}\frac{\exp(-\hbar\omega_l/2k_bT)}{1 - \exp(-\hbar\omega_l/k_bT)} \tag{5}$$

The correlation between the saturation pressure, $P_{sat}(T_I^L)$, and the local vapor-phase pressure, P_I^V, is given in eqs 1 to 5. Recent studies suggested that the measured global vapor-phase pressure cannot be treated as the local vapor-phase pressure if a thermocapillary flow is at an interface during the droplet evaporation.[13,14] Note that the local evaporation flux, the interfacial liquid and vapor temperatures, the radius of interface, and the molecular and thermal properties are known at each measured position. Therefore, the saturation pressure, $P_{sat}(T_I^L)$, could be predicted by an iterative calculation from the presetted values of the local vapor-phase pressure as shown in Figure 4. At each measured position, the initial local vapor-phase pressure was submitted into eqs 1 to 5 to calculate the saturation pressure which was compared with the pressures given from the equation of Pupezin et al., $P_{sat,P}$,[1] and the fitting relation from the data of Kraus and Greer, $P_{sat,KG(f)}$.[7] If the calculated saturation pressure from SRT was not between the values of $P_{sat,P}$ and $P_{sat,KG(f)}$, the iterative calculation with an increasing step was conducted until the criterion was satisfied. In the meanwhile, the local vapor-phase pressure would also be obtained. As illustrated in Figure 4a, the local vapor-phase pressure is uniform, as thermocapillary convection was not present at the interface in EVD3, for example. The measured global vapor-phase pressure agrees with the predicted vapor-phase pressure at each measured position. However, after the thermocapillary convection transition, the local vapor-phase pressure was not uniform any more along the evaporating interface. In the experiments of EVD11, it is found that the local vapor-phase pressure variation could be over 38.4 Pa from the centerline to 3.15 mm away from the centerline, although the average of the predicted vapor-phase pressures agrees with the measured global vapor-phase value in the measuring error bar. As seen in Figure 4b, the predicted saturation pressure is uniform locally in the experiment of EVD3 as the interface is quiescent, while the saturation pressure increases from the centerline to the edge of the evaporating droplet after the thermocapillary convection transition. After the local vapor-phase pressure, P_I^V, is determined in the nonequilibrium conditions, the local liquid-

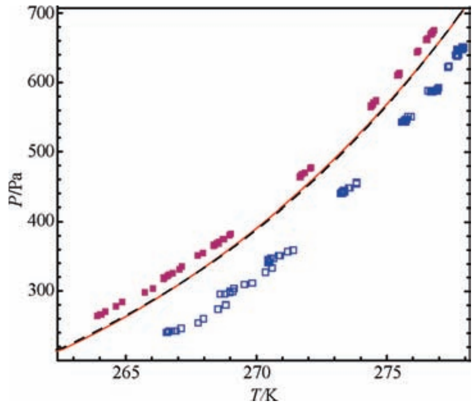

Figure 5. Comparison of the nonequilibrium pressures measured in the liquid phase (■) and vapor phase (□) during steady-state evaporation with the extrapolated saturation pressure from the fitting from Kraus and Greer data (black dashed line)[7] and Pupezin et al. (red solid line)[1] below the triple point at 275.97 K.

phase pressure, P_I^L, could be calculated at each measured position of the spherical droplet by using the Laplace equation.

$$P_I^L = P_I^V + \frac{2\gamma^{LV}}{R_0} \tag{6}$$

Under the steady-state evaporation conditions, the local vapor-phase pressure at the interfacial vapor temperature and the local liquid-phase pressure at the interfacial liquid temperature are plotted in Figure 5. It is found that the liquid-phase pressure and the vapor-phase pressure at the same measured position are on the either side of the extrapolated saturation pressure curve given by Pupezin et al.[1] The liquid-phase pressure is higher than the extrapolated saturated pressure at the same interfacial liquid temperature. The vapor-phase pressure is lower than the extrapolated saturation pressure at the same interfacial vapor temperature. It results from the effects of the curvature and the interfacial temperature discontinuity under the various local evaporation fluxes in the nonequilibrium processes. For example, at the centerline of the experiment of EVD11, the local vapor-phase pressure was 243.6 Pa under the interfacial vapor temperature at 266.64 K, while the local liquid-phase pressure was 267.0 Pa under the interfacial liquid temperature at 263.95 K. Thus, the vapor was superheated, and the liquid was subcooled during the evaporation. As a result of the effects of the local evaporation flux, several different values on the saturation pressure were observed at one temperature. As is well-known, the P_{sat} should be only one property at each interfacial liquid temperature under equilibrium.

The predicted saturation pressures from the SRT approach are plotted in Figure 6 as a function of the interfacial liquid temperature. If the predicted saturation pressures were compared with the fitting curve, as expressed in eq 7, it is found that the mean absolute derivation between the predicted saturation pressures and the fitting curve is within 0.31 %.

$$P_s(T) = 659.3 \exp[368.046 - 12146.9/T + 0.322999T - 4.11204 \cdot 10^{-4}T^2 + 3.48776 \cdot 10^{-7}T^3 - 1.32759 \cdot 10^{-10}T^4 - 69.1219 \ln T] \tag{7}$$

where P_{sat} is in Pa and T is in K.

Figure 7 demonstrates the relative variation between the fitting expression of the saturation pressure from SRT and the existing formulas proposed by Pupezin et al.,[1] Jones,[4] Bottomley,[5] Kraus and Greer,[6] Hill and MacMillan,[16] Harvey and Lemmon,[17] and Matsunaga and Nagashima.[18] The extension of the expression of Jones[4] below the triple point and the fitting equation of Bottomley[5] are away from the fitting curve from SRT in more than 2 %, which cannot be shown in Figure 7. The fitting equation of Kraus and Greer[6] indicates a departure of 5 % from eq 7 even if the part of curve is demonstrated. The other previous expressions shown in Figure 7 have small deviations, less than 0.45 %, from the SRT curve as they are extended into the temperature range from (250 to 283) K. To visualize the difference in the expression of P_{sat}, the specific enthalpy of evaporation, h_{fg}, of the heavy water was calculated to express the slopes of these pressure curves.

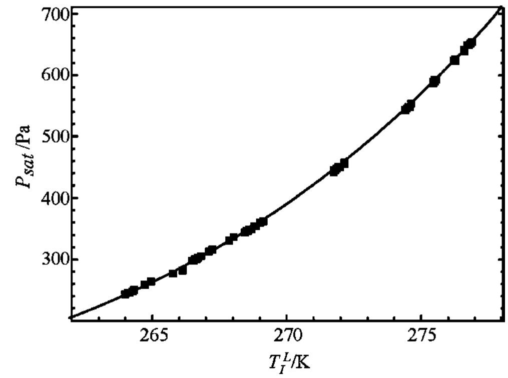

Figure 6. Predicted saturation pressure of D_2O from SRT compared with the fitting curve in eq 7.

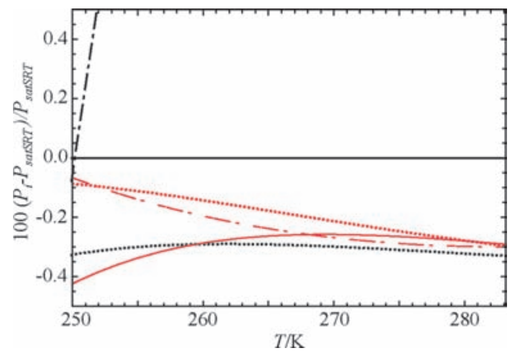

Figure 7. Comparison between the SRT fitting curve (black solid line) with the analytical expressions given by Pupezin et al. (red dashed−dotted line),[1] Kraus and Greer (black dashed−dotted line),[6] Hill and MacMillan (red solid line),[16] Harvey and Lemmon (red dashed line),[17] and Matsunaga and Nagashima (black dotted line).[18]

Calculation of the Specific Enthalpy of Evaporation of D_2O. The Gibbs−Duham equation gives,

$$s^L(T)\,dT + v^L\,dP_{sat} = s^V(T)\,dT + v^V\,dP_{sat} \tag{8}$$

where s^L or s^V is the specific entropy in the liquid or vapor phase, respectively, v^L or v^V is the specific volume in the liquid or vapor phase. After being simplified, the equation can be expressed as,

$$h_{fg} = T(v^V - v^L)\frac{dP_s}{dT} \tag{9}$$

where the specific enthalpy of evaporation, $h_{fg} = h^V - h^L$.

Since the vapor was in a superheated condition, it can be assumed as an ideal gas. As we know, the specific volume of D_2O vapor could be 10^5 times as that of the liquid at the triple

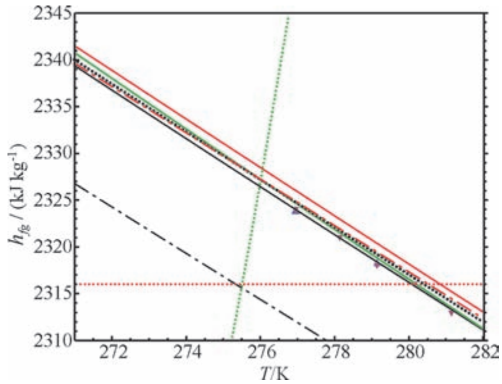

Figure 8. Comparison of the specific enthalpy of evaporation of D_2O in the present saturation pressure expression (black solid line) from the previous expression by Jones (black dashed−dotted line),[4] Bottomley (green dotted line),[5] Kraus and Greer (red dotted line),[6] Pupezin et al. (green solid line),[1] Hill and MacMillan (red dashed−dotted line),[16] Harvey and Lemmon (red solid line),[17] and Matsunaga and Nagashima (black dotted line)[18] and the measured values close to the triple point. Data from: ▼, Hill et al.;[19] △, Kazavchinskii and Kirillin.[20]

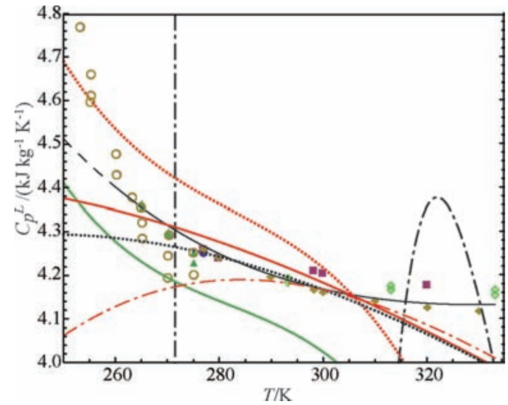

Figure 9. Comparison of the specific heat at constant pressure of D_2O in the liquid phase of present work (black solid line) from the experimental data and the formulation from Jones (green solid line),[4] Pupezin et al. (red dotted line),[1] Bottomley (black dashed-dotted line),[5] Hill and MacMillan (red dashed-dotted line),[16] Harvey and Lemmon (red solid line),[17] Matsunaga and Nagashima (black dotted line).[18] Data from: ○, Angell et al. (a);[25] ▲, Angell et al. (b);[25] ■, Braibanti et al.;[22] ◇, Rivkin and Egorov;[24] ◆, Smirnova et al.;[23] ●, John et al.[21]

point. Thus, the specific enthalpy of evaporation of D_2O could be expressed as,

$$h_{fg} = RT^2\frac{d\ln P_s}{dT} \qquad (10)$$

where R is the gas constant. After the equations for P_{sat} are substituted into eq 10, one may obtain an expression for h_{fg} corresponding to each expression for P_{sat}. The results obtained from this procedure are shown in Figure 8. The specific enthalpy of evaporation calculated from the expressions of the saturation pressure given by Jones,[4] Bottomley,[5] and Kraus and Greer[6] is clearly in disagreement with the reported data,[19,20] but the values of h_{fg} calculated from the expressions proposed by Pupezin et al.,[1] Hill and MacMillan,[16] Harvey and Lemmon,[17] and Matsunaga and Nagashima[18] differ from the measurements by less than 1 %. Importantly, the obtained SRT expression is almost in complete consistence with the measurements close to the triple point at 276.97 K.[19,20]

Calculation of the Specific Heat at Constant Pressure of D_2O in the Liquid Phase. After taking the further partial differential of the specific enthalpy of evaporation, h_{fg} with respect to T, one finds

$$C_p^L = C_p^V - 2RT\frac{d\ln P_s}{dT} - RT^2\frac{d^2\ln P_s}{dT^2} \qquad (11)$$

where C_p^V can been fitted from the data of Friedman and Haar[29] and expressed in eq 12 if T is the temperature in K.

$$C_p^V = 1.59376 + 1.52952\cdot 10^{-3}T + 1.18615\cdot 10^{-5}T^2 + 3.65264\cdot 10^{-8}T^3 + 3.02103\cdot 10^{-11}T^4 \qquad (12)$$

The values of C_p^L calculated from the expressions of P_{sat} given by Kraus and Greer,[6] Jones,[4] Pupezin et al.,[1] Bottomley,[5] Hill and MacMillan,[16] Harvey and Lemmon,[17] Matsunaga and Nagashima,[18] and the SRT expression are compared with the data measured by Jhon et al., Braibanti et al., Smirnova et al., Rivkin and Egorov, and Angell et al.,[21−25] as illustrated in Figure 9. The expression of C_p^L of Kraus and Greer is out of range in the plot, and the curves of Bottomley and Jones are clearly inconsistent with the measures. Although the variation of curves of Pupezin et al. from the SRT fitting curves is less than 0.45 % in P_{sat} and 1 % in h_{fg}, the variation of C_p^L could reach 5 % from the SRT curve and measured values. It is noticed that the equations of the saturation pressure of Pupezin et al., Hill and MacMillan, Harvey and Lemmon, Matsunaga and Nagashima, and Jones are all for the temperature range above the tripe point, but the calculated values of C_p^L from these expressions do not agree with the measures by Jhon et al.,[21] Braibanti et al.,[22] Rivkin and Egorov,[24] and Smirnova et al.[23] in the range from the triple point to 335 K. But the SRT analytical expression is agreeable with the measured values which have less than 1 % variation as indicated in Figure 9. Below the triple point, the two groups of measurements of C_p^L reported by Angell et al.,[25] one was read from the bulk samples, and another was obtained from the emulsion samples. There is almost no measurable difference between the SRT curve and the bulk measured values of Angell et al. The difference is less than 2 % in the temperature range above 260 K between the SRT calculated values and the emulsion data. However, the values of C_p^L obtained in an emulsion sample are greater than those calculated from the SRT equation from (250 to 260) K. The disagreement goes to above 4 % down to 250 K. In the temperature range, the SRT calculation is shown in a dashed line in Figure 9. Just as that in H_2O, Johari suggested that C_p^L had an unexpected larger increase in the emulsion technique with a decrease of temperature.[30] The statement agrees with the values of C_p^L calculated from the SRT equation (see Figure 9). On the other hand, while the temperature extends down to 250 K, there is significant disagreement between the measures of C_p^L and calculated values from the equations of saturation pressure of Pupezin et al.,[1] Jones,[4] Hill and MacMillan,[16] Harvey and Lemmon,[17] or Matsunaga and Nagashima.[18]

Thus, the thermal properties of D_2O were determined from the SRT expression in nonequilibrium evaporation, in which a temperature discontinuity was found at the evaporation interface. The predictions of h_{fg} and C_p^L from the SRT expression are consistent with the independent measurements. It suggests that the SRT approach could be applied to predict the saturation pressure, P_{sat}, the specific entropy of evaporation, h_{fg}, and the liquid-phase specific heat at constant pressure, C_p^L, for D_2O near the triple point at a nonequilibrium interface.

Conclusions

The nonequilibrium process between the liquid and the vapor phases was demonstrated in Figure 3 with the interfacial vapor temperature higher than the interfacial liquid temperature. The temperature discontinuity was up to 2.7 K in the experiment of EVD11. The nonequilibrium could also be evaluated from $(P_{sat}(T_I^V) - P_{sat}(T_I^L))$ with the help of eq 7. The saturation pressure difference at the centerline is 48.1 Pa for EVD1 and 58.6 Pa for EVD11. In 102 local evaporation measurements of D_2O, the saturation pressure, P_{sat}, as a function of measured interfacial liquid temperature, T_L^I, was predicted numerically in the SRT approach in terms of the measurable interfacial temperatures and the local evaporation flux over a range of temperature near the triple point. An expression for P_{sat} determined experimentally is given in eq 7 and shown in Figure 6 along with the data obtained from the steady-state nonequilibrium evaporation interfaces. The vapor-phase pressure as a function of the interfacial vapor temperature is not overlapped with the liquid-phase pressure as a function of the interfacial liquid temperature as shown in Figure 5. However, the expression for P_{sat} obtained from the SRT approach in a nonequilibrium process is more accurate in predicting the values of h_{fg} and C_p^L than the other existing ones. If the vapor is assumed as an ideal gas, the predictions of h_{fg} and C_p^L obtained from SRT and other existing analytical expressions of P_{sat} are compared with the independent measurements of these properties. The predicted values of h_{fg} obtained from the different expressions for P_{sat} are shown in Figure 8, where only the SRT expression for h_{fg} is in complete agreement with the reported data. The SRT expression for C_p^L is also the only one consistent with the measured data at the temperatures down to 260 K (Figure 9). Although the vapor-phase pressure as a function of the interfacial vapor temperature is not overlapped with the liquid-phase pressure as a function of the interfacial liquid temperature as shown in Figure 5, the expression for P_{sat} obtained from the SRT approach in a nonequilibrium process is more accurate in predicting the values of h_{fg} and C_p^L than the other existing ones.

Acknowledgment

F.D. wishes to acknowledge the support of Prof. C. A. Ward when he worked there.

Literature Cited

(1) Pupezin, J.; Jakli, G.; Jansco, G.; Van Hook, W. A. Vapor pressure isotope effect in aqueous systems. I. Water-water-d_2 (−64 deg to 100 deg) and water-water 18-0 (−17 deg to 16 deg). Ice and liquid. II. Alkali metal chloride solution in water and water-d_2 (−5 deg to 100 deg). *J. Phys. Chem.* **1972**, *76*, 743–762.
(2) Besiey, L.; Bottomley, G. A. Vapour pressure of normal and heavy water from 273.15 to 298.15 K. *J. Chem. Thermodyn.* **1973**, *5*, 397–410.
(3) Jakli, G.; Van Hook, W. A. Vapor pressure of heavy water at 283−363 K. *J. Chem. Eng. Data* **1981**, *26*, 243–245.
(4) Jones, W. M. Interpretation of the isotope effects. *J. Chem. Phys.* **1968**, *48*, 207–214.
(5) Bottomley, G. A. The vapour pressure of supercooled water and heavy water. *Aust. J. Chem.* **1978**, *31*, 1177–1180.
(6) Kraus, G. F.; Greer, S. C. Vapor pressures of supercooled H_2O and D_2O. *J. Phys. Chem.* **1984**, *88*, 4781–4785.
(7) Duan, F.; Ward, C. A. Surface-thermal capacity of D_2O from measurements made during steady-state evaporation. *Phys. Rev. E* **2005**, *72*, 056304.
(8) Ward, C. A.; Fang, G. Expression for predicting liquid evaporation flux: Statistical rate theory approach. *Phys. Rev. E* **1999**, *59*, 429–440.
(9) Duan, F.; Thompson, I.; Ward, C. A. Statistical rate theory determination of water properties below the triple point. *J. Phys. Chem. B* **2008**, *112*, 8605–8613.
(10) Ward, C. A. Liquid-vapour phase change rates and interfacial entropy production. *J. Non-Equilib. Thermodyn.* **2002**, *27*, 289–303.
(11) Duan, F.; Badam, V. K.; Durst, F.; Ward, C. A. Thermocapillary transport of energy during water evaporation. *Phys. Rev. E* **2005**, *72*, 056303.
(12) Duan, F.; Ward, C. A.; Badam, V. K.; Durst, F. Role of molecular phonons and interfacial-temperature discontinuities in water evaporation. *Phys. Rev. E* **2008**, *78*, 041130.
(13) Duan, F. Local evaporation flux affected by thermocapillary convection transition at an evaporating droplet. *J. Phys. D: Appl. Phys.* **2009**, *42*, 102004.
(14) Duan, F.; Ward, C. A. Investigation of local evaporation flux and vapor-phase pressure at an evaporative droplet interface. *Langmuir* **2009**, *25*, 7424–7431.
(15) Thompson, I.; Duan, F.; Ward, C. A. Absence of Marangoni convection at Marangoni numbers above 27,000 during water evaporation. *Phys. Rev. E* **2009**, *80*, 056308.
(16) Hill, P. G.; MacMillan, R. D. C. A saturation vapor pressure equation for heavy water. *Ind. Eng. Chem. Fundam.* **1979**, *18*, 412–415.
(17) Harvey, A. H.; Lemmon, E. W. Correlation for the vapor pressure of heavy water from the triple point to the critical point. *J. Phys. Chem. Ref. Data* **2002**, *31*, 173–181.
(18) Matsunaga, N.; Nagashima, A. Saturation vapor pressure and critical constants of H_2O, D_2O, T_2O, and their isotopic mixtures. *Int. J. Thermophys.* **1987**, *8*, 681–694.
(19) Hill, P. G.; MacMillan, R. D. C.; Lee, V. A fundamental equation of state for heavy water. *J. Phys. Chem. Ref. Data* **1982**, *11*, 1–14.
(20) Kazavchinskii, Y. Z.; Kirillin, V. A. *Heavy Water - Thermophysical Properties*; Jerusalem Israel Program for Scientific Translations: Jerusalem, 1971.
(21) Jhon, M. S.; Grosh, J.; Ree, T.; Eyring, H. Significant-structure theory applied to water and heavy water. *J. Chem. Phys.* **1966**, *44*, 1465–1472.
(22) Braibanti, A.; Fisicaro, E.; Ghiozzi, A.; Compari, C. Isobaric heat capacity and structure of water and heavy water in the liquid state. *Thermochim. Acta* **1996**, *286*, 51–66.
(23) Smirnova, N. N.; Bykova, T. A.; Van Durme, K.; Van Mele, B. Thermodynamic properties of deuterium oxide in the temperature range from 6 to 350 K. *J. Chem. Thermodyn.* **2006**, *38*, 879–883.
(24) Rivkin, S. L.; Egorov, B. N. The specific heat of heavy water. *J. Nucl. Energy, Parts A/B* **1961**, *14*, 137–139.
(25) Angell, C. A.; Oguni, M.; Sichina, W. J. Heat capacity of water at extremes of supercooling and superheating. *J. Phys. Chem.* **1982**, *86*, 998–1002.
(26) Ward, C. A.; Duan, F. Turbulent transition of thermocapillary flow induced by water evaporation. *Phys. Rev. E* **2004**, *69*, 056308.
(27) Duan, F.; Ward, C. A. Surface excess properties from energy transport measurements during water evaporation. *Phys. Rev. E* **2005**, *72*, 056302.
(28) Lemus, R. Vibrational excitations in H_2O in the framework of a local model. *J. Mol. Spectrosc.* **2004**, *225*, 73–92.
(29) Friedman, A. S.; Haar, L. High-speed machine computation of ideal gas thermodynamic functions. I. Isotopic water molecules. *J. Chem. Phys.* **1954**, *22*, 2051–2058.
(30) Johari, G. P. The Gibbs-Thomson effect and intergranular melting in ice emulsions: Interpreting the anomalous heat capacity and volume of supercooled water. *J. Chem. Phys.* **1997**, *107*, 10154–10165.

Received for review March 10, 2010. Accepted June 3, 2010. The study is supported from AcRF TIER1 funding (M52050110).

JE100226G